

FTO-mediated demethylation of GADD45B promotes myogenesis through the activation of p38 MAPK pathway

Kaiping Deng,¹ Yixuan Fan,¹ Yaxu Liang,¹ Yu Cai,¹ Guomin Zhang,¹ Mingtian Deng,¹ Zhibo Wang,¹ Jiawei Lu,¹ Jianfei Shi,² Feng Wang,^{1,3} and Yanli Zhang¹

¹Institute of Sheep and Goat Science, Nanjing Agricultural University, Nanjing 210095, China; ²Haimen Goat Breeding Farm, Nantong 226100, China; ³Institute of Haimen Goat Industry, Nanjing Agricultural University, Nanjing 210095, China

N6-methyladenosine (m⁶A) modification plays a critical role in mammalian development. However, the role of m⁶A in the skeletal muscle development remains largely unknown. Here, we report a global m⁶A modification pattern of goat skeletal muscle at two key development stages and identified that the m⁶A modification regulated the expression of the growth arrest and DNA damage-inducible 45B (*GADD45B*) gene, which is involved in myogenic differentiation. We showed that *GADD45B* expression increased during myoblast differentiation, whereas the downregulation of *GADD45B* inhibits myogenic differentiation and mitochondrial biogenesis. Moreover, the expression of *GADD45B* regulates the expression of myogenic regulatory factors and peroxisome proliferator-activated receptor gamma coactivator 1 alpha by activating the p38 mitogen-activated protein kinase (MAPK) pathway. Conversely, the inactivation of p38 MAPK abolished the *GADD45B*-mediated myogenic differentiation. Furthermore, we found that the knockdown of fat mass and obesity-associated protein (FTO) increases *GADD45B* m⁶A modification and decreases the stability of *GADD45B* mRNA, which impairs myogenic differentiation. Our results indicate that the FTO-mediated m⁶A modification in *GADD45B* mRNA drives skeletal muscle differentiation by activating the p38 MAPK pathway, which provides a molecular mechanism for the regulation of myogenesis via RNA methylation.

INTRODUCTION

Skeletal muscle is an indispensable component of the body, playing a vital role in locomotion, metabolism, and homeostasis. It originates from mesodermal progenitors, which undergo a complex, multistep process of myoblast proliferation and fusion, myotube formation, and myofiber maturation during embryogenesis.^{1,2} Skeletal muscle development, also called myogenesis, occurs as a result of the coordination of complex transcriptional regulatory networks, consisting of myogenic regulatory factors (MRFs), the myocyte enhancer factor 2 family, and other related transcription factors, as well as several signaling molecules, such as mitogen-activated protein kinase (MAPK), Wnt, and transforming growth factor- β (TGF- β).^{1,3-5}

Moreover, post-transcriptional regulation also contributes to myogenesis via RNA binding proteins and noncoding RNAs.⁶⁻⁸ Although mRNA modifications play key roles in post-transcriptional gene regulation,⁹ their roles in regulating myogenesis and the underlying mechanisms remain unclear.

More than 150 types of chemical modifications have been identified in cellular RNAs.¹⁰ Among these, N6-methyladenosine (m⁶A) modification has attracted the most attention because of its prevalence and biological functions in mammals.¹¹⁻¹³ The m⁶A modification of mRNA is a reversible process that is dynamically regulated by m⁶A writers and erasers. The m⁶A writer complex consists of methyltransferase-like 3 (METTL3), methyltransferase-like 14 (METTL14), and Wilms tumor 1-associated protein (WTAP), which can catalyze the methylation of specific adenosines in mammalian mRNA.^{14,15} Fat mass and obesity-associated protein (FTO) and alpha-ketoglutarate-dependent dioxygenase alkB homolog 5 (ALKBH5) have been identified as m⁶A erasers, in which their role is to remove m⁶A modifications.¹⁶ m⁶A modifications have been shown to exert important functions in stem cell self-renewal and differentiation, cell fate determination, tissue development, carcinogenesis, and stress response regulation, as well as in RNA metabolism, including mRNA stability, splicing, transport, localization, and translation.¹⁷⁻²⁰ Recent *in vivo* studies have led to breakthroughs in elucidating the effects of m⁶A modifications on mammalian development. Aberrant m⁶A modifications were found to impair cell-cycle progression, stem cell differentiation, bone homeostasis balance, and brown adipogenesis and to retard neurogenesis.²¹⁻²³ It has also been reported that *FTO* knockout in mice reduces the volume of lean body mass,^{24,25} therefore, it is crucial to understand the potential role of m⁶A modifications in skeletal muscle development in large animals, such as goats.

Received 11 November 2020; accepted 14 June 2021;
<https://doi.org/10.1016/j.omtn.2021.06.013>.

Correspondence: Feng Wang, PhD, Institutes of Sheep and Goat Science and Haimen Goat Industry, Nanjing Agricultural University, Nanjing 210095, China.
E-mail: caee@njau.edu.cn

Correspondence: Yanli Zhang, PhD, Institute of Sheep and Goat Science, Nanjing Agricultural University, Nanjing 210095, China.
E-mail: zhangyanli@njau.edu.cn

Here, we explored the RNA m⁶A modification profile of goat skeletal muscle at key developmental stages (75-day fetus, 1-day-old kid) and identified growth arrest and DNA damage-inducible 45B (*GADD45B*) as a potential m⁶A-mediated gene involved in myogenesis. Importantly, the molecular mechanism underlying the role of *GADD45B* in myogenic differentiation and the effect of m⁶A modifications on *GADD45B* expression were also investigated. Taken together, our findings demonstrate that *GADD45B* expression is regulated by FTO-mediated m⁶A modification and promotes myogenic differentiation by activating the p38 MAPK pathway.

RESULTS

m⁶A levels decreased during myogenic differentiation *in vivo* and *in vitro*

To determine the potential role of m⁶A modification in myogenesis, we evaluated the correlation between the m⁶A content and myogenic differentiation *in vivo*. First, the muscle collected from goats at different developmental stages was physiologically investigated. The size and number of myofibers in newly born kid skeletal muscle were markedly higher compared with that of myofibers in the fetal skeletal muscle (Figures 1A and 1B). Furthermore, based on the ImageJ analysis (National Institutes of Health, Bethesda, MD, USA) of the H&E staining of the longissimus muscle, it was found that the number of myofibers occupying a larger area (>80 μm² in area) was higher in the kid samples than in the fetus samples, whereas the number of smaller-sized myofibers (<80 μm² in area) was significantly lower in the kid samples than in the fetus samples (Figure 1C). This corresponds to the muscular development phenotype of the two development stages. The myogenic differentiation marker actin, alpha skeletal muscle (*ACTA1*) was significantly upregulated in the kids compared to the fetuses; in contrast, the expression of paired box 7 (*PAX7*), the gene responsible for the maintenance of satellite cells, was reduced during development (Figure 1D).

Next, colorimetry was used to quantify the global m⁶A modifications in skeletal muscle during the embryonic period and at the newborn stage.²⁶ As a result, fewer global m⁶A modifications were observed in the muscles of kids compared to those of fetuses (Figure 1E). Consistently, m⁶A demethylase FTO was more highly expressed in kid muscle samples than in fetal muscle samples, whereas the expression of m⁶A methyltransferase METTL3 was lower in kid muscle samples than in fetal muscle samples (Figure 1F).

Furthermore, we sought to explore the correlation between m⁶A modifications and myogenic differentiation *in vitro*. Goat primary myoblasts (GPMs) were isolated, identified, and differentiated (Figures 1G and S1). Consistently, the level of global m⁶A modifications decreased markedly, along with the differentiation of GPMs (Figure 1H). In line with this finding, the expression of FTO increased, along with the myogenic differentiation of GPMs, whereas the level of METTL3 decreased after differentiation initiation (Figure 1I). These results indicate that m⁶A modifications may negatively regulate myogenesis.

Identification of *GADD45B* as a potential m⁶A-modified gene related to myogenesis

To identify the potential m⁶A-modified genes related to myogenesis, the m⁶A distribution in fetal (75 days) and kid (newborn stage) skeletal muscle was analyzed. First, the m⁶A methylomes of fetal and kid skeletal muscle were mapped using m⁶A sequencing (m⁶A-seq) and four biological replicates. As shown in Table S1, 64.0 to 111.1 million reads were obtained from each m⁶A-seq or RNA sequencing (RNA-seq) library. Consistent with the published consensus motif RRACH (R = G or A; H = A, C or U),¹¹ the GGACU sequence was identified as the most common m⁶A motif in goat skeletal muscle (Figure 2A). Notably, a total of 4,632 and 2,789 m⁶A peaks from 3,270 to 2,227 m⁶A-modified transcripts in fetal and kid skeletal muscle were identified using m⁶A-seq, respectively (Figures 2B and 2C). In kid skeletal muscle, 1,654 new peaks appeared, whereas 3,498 peaks disappeared. The other 1,134 peaks were observed in both fetal and kid skeletal muscle (Figure 2B). Furthermore, the m⁶A peak distribution patterns within the whole transcripts were investigated. The m⁶A peaks mainly appeared in the coding sequence (CDS) and 3' UTR regions and were especially abundant close to the stop codon (Figures 2D and S2A). A total of 937 common m⁶A-modified genes were identified in both fetal and kid muscle, and 2,333 and 1,290 unique m⁶A-modified genes were observed in fetal and kid skeletal muscle, respectively (Figure 2C). With the use of Gene Ontology (GO) enrichment and Kyoto Encyclopedia of Genes and Genomes (KEGG) pathway analysis, the m⁶A-modified genes were found to be mainly involved in focal adhesion, actin binding, actin filament binding, and myotube differentiation, as well as in some signaling pathways related with skeletal muscle development, including the MAPK and Wnt signaling pathways (Figures S2B and S2C).

Next, we compared the m⁶A peak abundance of common m⁶A-modified genes between the skeletal muscle of fetuses and kids. A total of 185 hyper-methylated m⁶A peaks and 372 hypo-methylated m⁶A peaks were discovered in the kid skeletal muscles relative to the fetal skeletal muscles (fold change >1.5, *p* < 0.05; Figure 2E; Table S2). With the use of cross analysis of the m⁶A-seq and RNA-seq data, we identified 109 hyper-methylated m⁶A peaks in the mRNA transcripts, which were significantly (fold change >1.5, *p* < 0.05) upregulated (107; hyper up) or downregulated (2; hyper down) in the kid skeletal muscle relative to the fetal skeletal muscle (Figure 2F; Table S3). Moreover, 222 hypo-methylated m⁶A peaks in the mRNA transcripts were found to be significantly (fold change >1.5, *p* < 0.05) upregulated (3; hypo up) or downregulated (209; hypo down) (Figure 2F; Table S3). Interestingly, based on the results of the associated analysis of m⁶A peak abundance and the mRNA transcripts levels, a positive correlation was found between the differentially methylated m⁶A peaks and the gene expression levels in these common m⁶A-modified genes (Figure 2G). Therefore, given the potentially negative correlation between m⁶A modifications and myogenesis, hypo-methylated genes were considered as candidate genes in the regulation of muscle development. Notably, only three upregulated genes were found among these hypo-methylated transcripts, one of which, *GADD45B*, is involved in myogenesis²⁷ and could activate

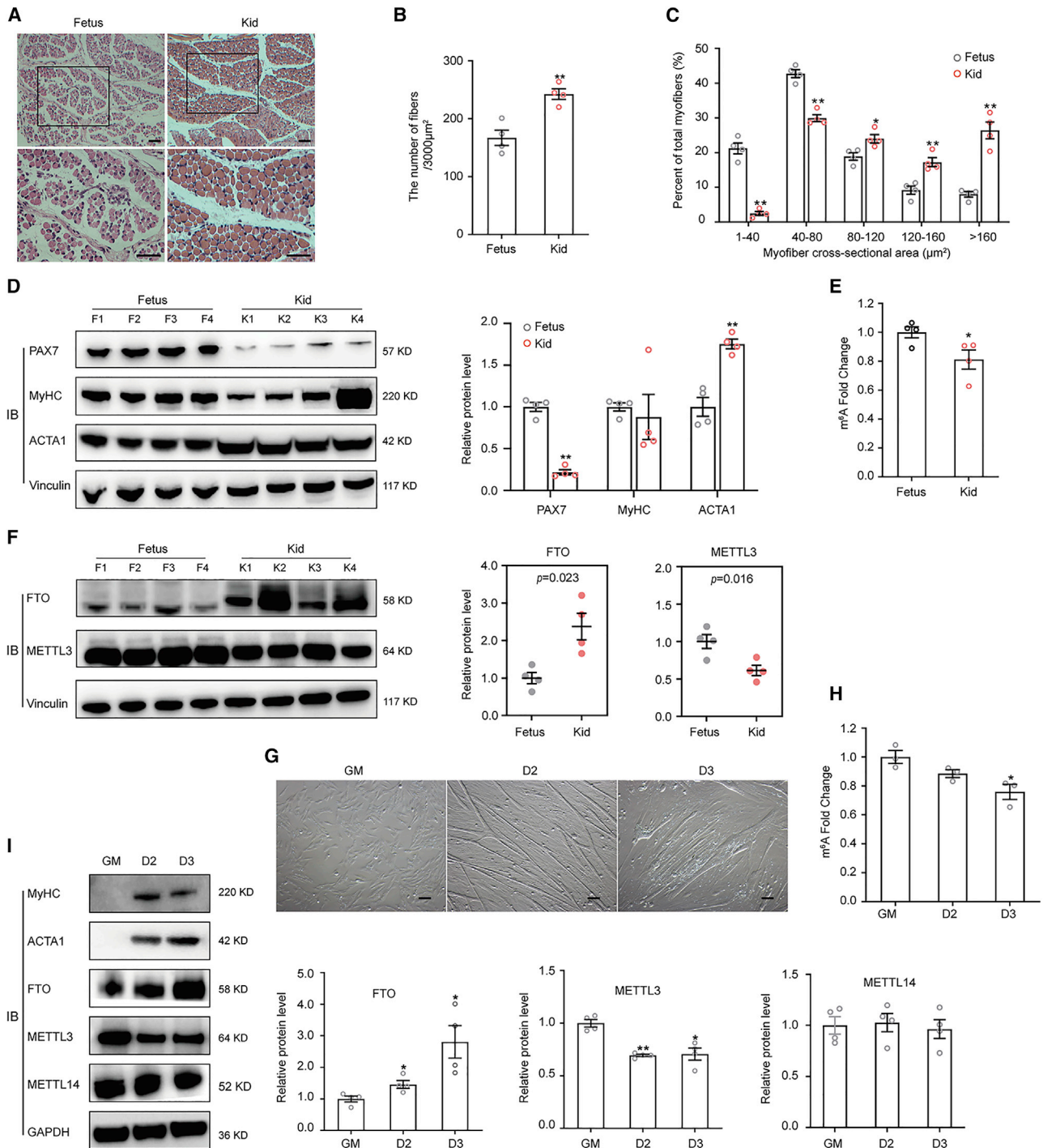


Figure 1. m⁶A levels decreased during myogenic differentiation *in vivo* and *in vitro*

(A) H&E analysis of longissimus muscle from fetuses and kids. Scale bars, 50 μm . The number of muscle fibers (B) was determined, and the distribution of fiber sizes (C) was analyzed. (D) Western blot analysis of myogenic differentiation markers in the longissimus muscle from fetuses and kids. (E) m⁶A levels in longissimus muscle from fetuses and kids. (F) Western blot analysis of FTO and METTL3 in longissimus muscle from fetuses and kids. (G–I) GPMs were differentiated for 3 days in differentiation medium. (G) Phase contrast microscopy images of GPMs at days 0 (growth medium [GM]), 2 (D2), and 3 (D3) of differentiation. Scale bars, 50 μm (H) m⁶A levels in differentiating GPMs. (I) Western blot analysis of MyHC, ACTA1, FTO, METTL3, and METTL14 in differentiating GPMs. The data were obtained from at least three independent experiments. Values are expressed as the mean \pm SEM; * $p < 0.05$, ** $p < 0.01$.

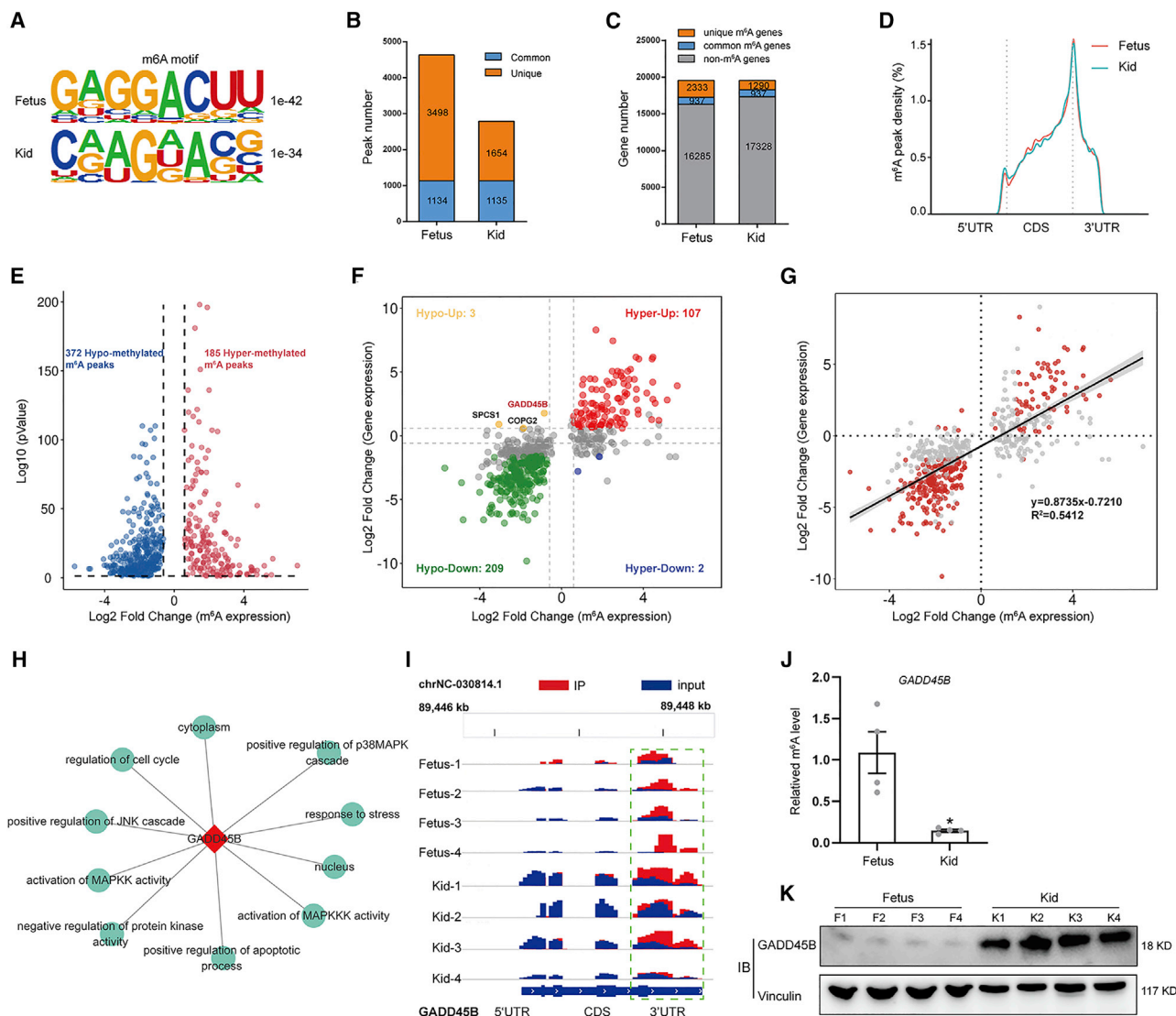


Figure 2. Identification of *GADD45B* as a potential m⁶A-modified gene involved in myogenesis using m⁶A-seq and RNA-seq

(A) Identification of the top consensus motif from m⁶A peaks identified in the skeletal muscle from fetuses and kids. (B) Number of m⁶A peaks identified using m⁶A-seq in the skeletal muscle from fetuses and kids. (C) Summary of the m⁶A-modified genes identified using m⁶A-seq. Common m⁶A genes contain at least one common m⁶A peak, whereas unique m⁶A genes contain no common m⁶A peaks. (D) Distribution of m⁶A peaks across transcripts divided into three segments: 5' UTR, CDS, and 3' UTR. (E) Identification of abundance of 372 hyper-methylated and 185 hypo-methylated m⁶A peaks that displayed a significant increase or decrease (fold-change >1.5; p < 0.05), respectively, in the skeletal muscle of kids relative to that of fetuses. (F) Distribution of genes with a significant change in both the mRNA and m⁶A modification levels in the skeletal muscle of kids relative to that of fetuses. (G) Correlation analysis between the abundance of m⁶A peaks and the expression level of their associated transcripts in the skeletal muscle of fetuses and kids. (H) GO term network of *GADD45B*. (I) The m⁶A abundance in *GADD45B* mRNA transcripts in skeletal muscle from fetuses and kids, as detected using m⁶A-seq. (J) m⁶A quantitative real-time PCR analysis of the m⁶A level of *GADD45B* mRNA in the skeletal muscle of fetuses and kids. (K) Western blot analysis of the *GADD45B* protein level in the skeletal muscles of fetuses and kids. The data were obtained from at least three independent experiments. Values are expressed as the mean ± SEM; *p < 0.05, **p < 0.01.

the MAPK pathway to regulate cell cycle and apoptosis (Figure 2H). The m⁶A-seq data showed that *GADD45B* contained m⁶A sites in the 3' UTR, with the m⁶A levels at 3' UTR markedly lower in the kid skeletal muscle compared to the fetal skeletal muscle (Figure 2I). In line with the m⁶A-seq data, the m⁶A quantitative real-time PCR results further confirmed that the m⁶A level in

GADD45B 3' UTR was lower in the kid skeletal muscle than in the fetal skeletal muscle (Figure 2J). Notably, *GADD45B* expression was found to be markedly upregulated during skeletal muscle development (Figure 2K). These results suggest that *GADD45B* is a m⁶A-modified gene with the potential function of regulating skeletal muscle development.

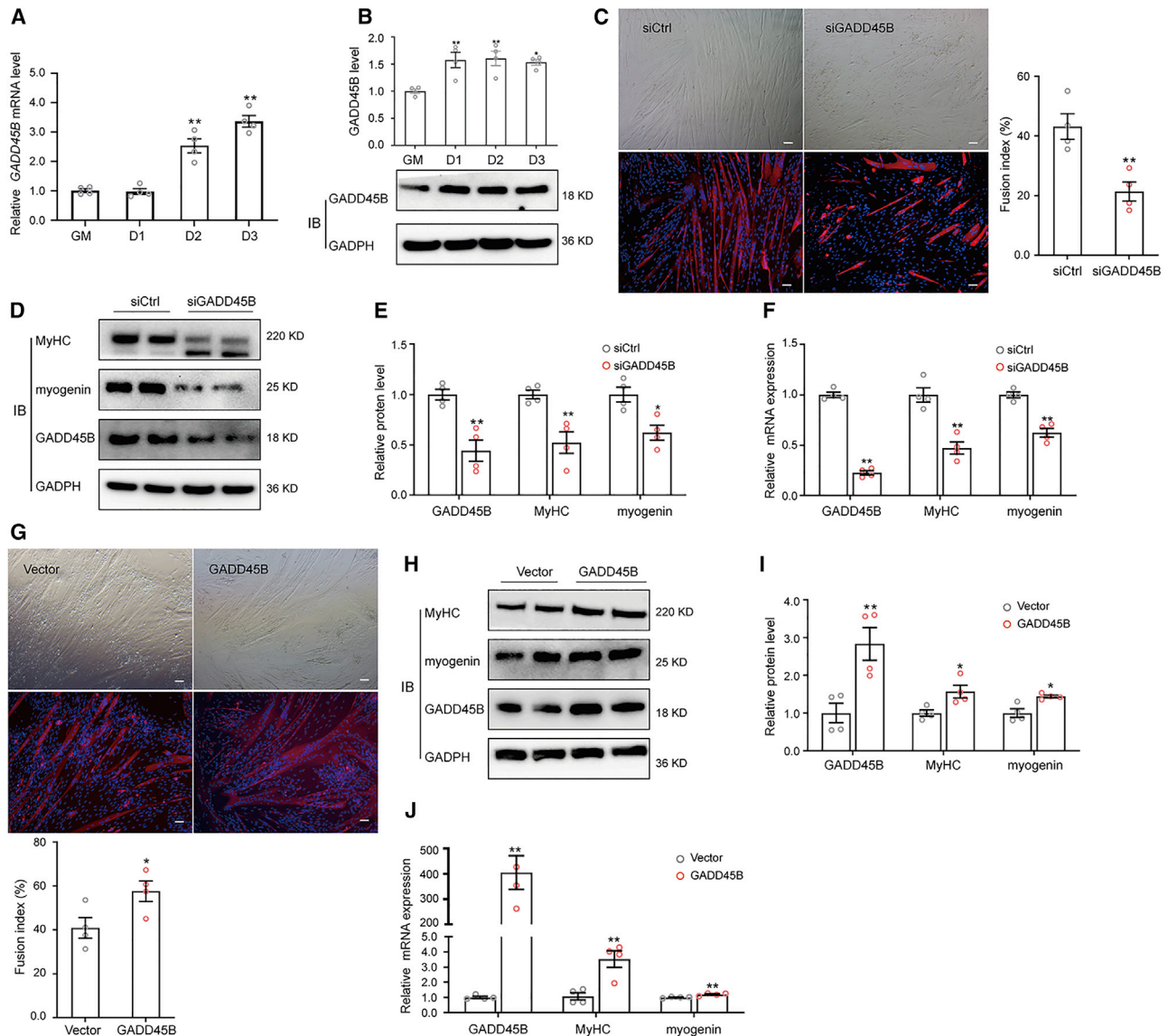


Figure 3. GADD45B regulates myogenesis *in vitro*

GPMs were differentiated for 3 days in differentiation medium. The mRNA (A) and protein (B) expression levels of GADD45B in differentiating GPMs, as determined using quantitative real-time PCR and western blotting. (C–F) After transfection with control siRNA (siCtrl) or GADD45B siRNA (siGADD45B), the differentiation of GPMs was induced for 3 days. (C) Representative images (left) of myotube formation in differentiated siCtrl and siGADD45B cells. Scale bars, 50 μ m. Cells were stained with DAPI (blue) and Ab11083 (red) to image the nuclei and MyHC, respectively. Quantitative analysis of the fusion index (right). The protein (D) and mRNA (F) expression levels of GADD45B, MyHC, and myogenin in differentiated siCtrl and siGADD45B cells, as detected using western blot and quantitative real-time PCR. (E) Quantitation of the western blot results of (D). (G–J) After transfection with the pEX3 plasmid (Vector) and pEX3-GADD45B plasmid (GADD45B), the differentiation of GPMs was induced for 3 days. (G) Representative images (top) of myotube formation in the differentiated vector and GADD45B cells. Scale bars, 50 μ m. Quantitative analysis of the fusion index (bottom). The protein (H) and mRNA (J) expression levels of GADD45B, MyHC, and myogenin in the differentiated vector and GADD45B cells, as detected using western blot and quantitative real-time PCR. (I) Quantitation of the western blot results of (H). The data were obtained from at least three independent experiments. The values are expressed as the mean \pm SEM; * p < 0.05, ** p < 0.01.

GADD45B affects myogenic differentiation and myoblast mitochondria biogenesis

To demonstrate the fact that *GADD45B* is a m⁶A-modified gene and regulates myogenesis, the function of *GADD45B* in myogenesis was explored. First, we measured the levels of *GADD45B* mRNA and

protein, both of which were found to increase during myogenic differentiation (Figures 3A and 3B), further suggesting that *GADD45B* has a potential function in myogenesis. Interestingly, the depletion of *GADD45B* using small interfering RNA (siRNA) was found to dramatically suppress the formation of myotubes during

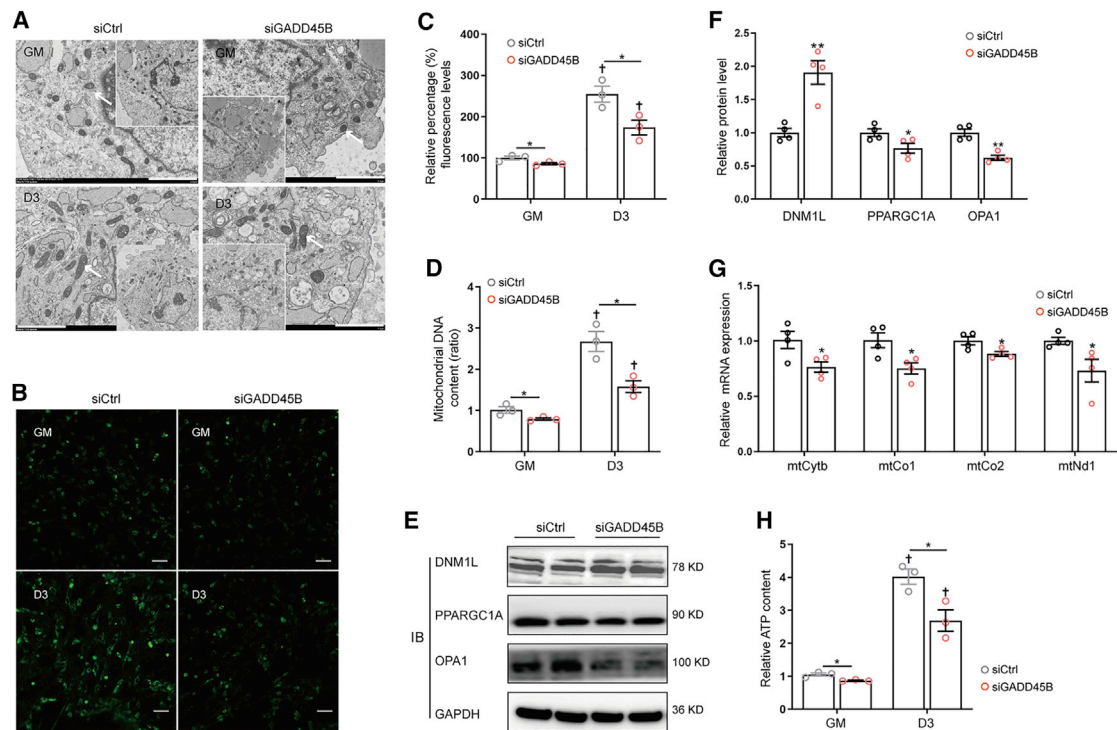


Figure 4. Depletion of GADD45B impairs mitochondria biogenesis and function during myogenic differentiation

(A) Electron micrographs of siCtrl and siGADD45B cells at GM and D3 of differentiation. Scale bars, 2 μ m. (B) Fluorescent images of Mito-Tracker Green stained siCtrl and siGADD45B cells at GM and D3 of differentiation. Scale bars, 50 μ m. (C) The fluorescence intensity quantification of Mito-Tracker Green in siCtrl and siGADD45B cells at GM and D3 of differentiation, as detected using a fluorescence microplate reader. (D) Mitochondrial DNA copy number in siCtrl and siGADD45B cells at GM and D3 of differentiation. (E) Western blot analysis of DNM1L, PPARGC1A, and OPA1 in siCtrl and siGADD45B cells at D3 of differentiation. (F) Quantitation of the western blot results of (E). (G) Quantitative real-time PCR analysis of the expression of mitochondrial DNA-encoded genes in siCtrl and siGADD45B cells at D3 of differentiation. (H) ATP levels in siCtrl and siGADD45B cells at GM and D3 of differentiation. The data were obtained from at least three independent experiments. The values are expressed as the mean \pm SEM; * p < 0.05 compared with GM; * p < 0.05 and ** p < 0.01 between groups at the same time point.

differentiation (Figure 3C). Consistently, the protein abundance and the mRNA level of myosin heavy chain (MyHC) and myogenin were markedly decreased upon GADD45B depletion (Figures 3D–3F). In contrast, the overexpression of GADD45B promoted the formation of myotubes during differentiation (Figure 3G). Moreover, the forced expression of GADD45B significantly increased the protein and mRNA expression of MyHC and myogenin (Figures 3H–3I).

Given that mitochondrial remodeling is required for the differentiation of myoblasts into myotubes and that GADD45B may affect mitochondria biogenesis in brown adipocytes,^{28–30} we sought to determine whether GADD45B plays a role in mitochondria biogenesis during myogenic differentiation. Transmission electron microscopy was used to detect the status of mitochondrial networks in differentiating cells. Electron micrographs showed that the mitochondrial populations were relatively dense and exhibited an elongated morphology in differentiated myoblasts compared to undifferentiated myoblasts (Figure 4A). However, in differentiated myoblasts lacking GADD45B, mitochondria are sparse and mostly round (Figure 4A). Moreover, the analysis of the mitochondrial mass (Figures 4B and 4C) and mitochondrial DNA content (Figure 4D) indicated that

mitochondrial biogenesis was repressed upon GADD45B depletion during myogenic differentiation. Interestingly, upon GADD45B deficiency, the protein level of mitochondrial fission protein dynamin 1 like (DNM1L) was elevated, whereas the protein levels of mitochondrial biogenesis-related protein peroxisome proliferator-activated receptor gamma coactivator 1-alpha (PPARGC1A) and mitochondrial fusion protein OPA1 were decreased (Figures 4E and 4F). In addition, GADD45B depletion resulted in the downregulation of mitochondrial-encoded genes (*mtCytb*, *mtCo1*, *mtCo2*, and *mtNd1*) in GPMs (Figure 4G), as well as in a reduction in the ATP levels during differentiation (Figure 4H). To further assess the influence of mitochondrial dysfunction caused by GADD45B deficiency on cellular homeostasis, we examined the levels of cell autophagy and apoptosis. Reactive oxygen species (ROS) production, autophagy related 7 (ATG7) and autophagy related 5 (ATG5) expression, and the microtubule-associated protein 1 light chain 3 β -II/I (LC3B-II/I) ratio were elevated in GADD45B-depleted cells than in control cells (Figures S3A–S3D). Meanwhile, the expression of autophagic adaptor protein sequestosome 1 (SQSTM1) was reduced (Figures S3C and S3D), which indicated that GADD45B deficiency elevated the level of autophagy GPMs at day 3 of differentiation. Moreover,

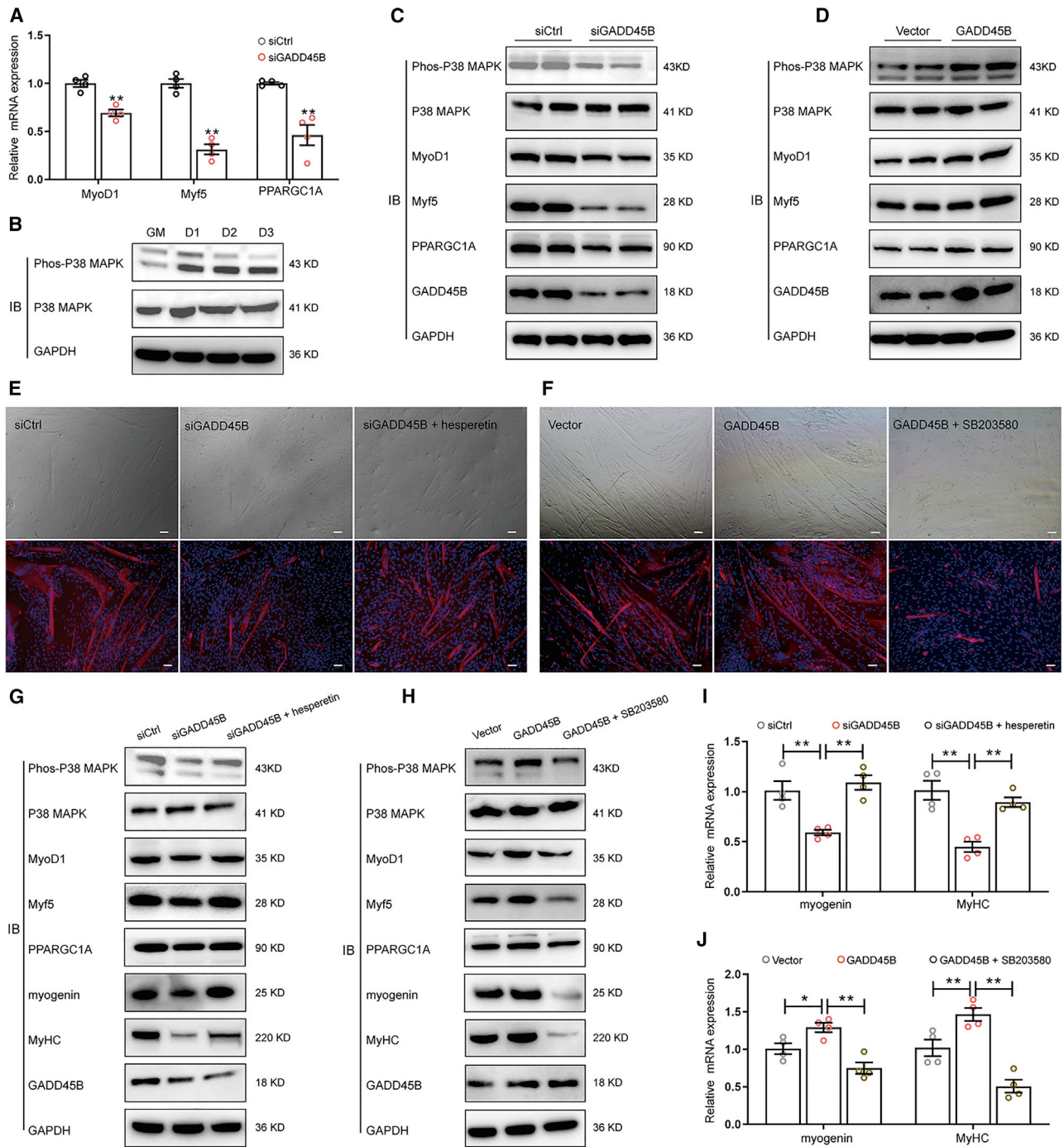


Figure 5. The p38 MAPK pathway is crucial for GADD45B-mediated myogenic differentiation

(A) Quantitative real-time PCR analysis of the expression of *MyoD1*, *Myf5*, and *PPARGC1A* in siCtrl and siGADD45B cells at D3 of differentiation. (B) Western blot analysis of the levels of phosphorylation and non-phosphorylation of p38 MAPK in differentiating GPMs. (C and D) Western blot analysis of the level of phosphorylation and non-phosphorylation of p38 MAPK, MyoD1, Myf5, and PPARGC1A in GADD45B knockdown (C) and GADD45B overexpression (D) GPMs at D1 of differentiation. (E–J) After transfection with GADD45B siRNA or the pEX3-GADD45B plasmid, GPMs were treated with 40 nM hesperetin or 10 nM SB203580 in differentiation medium for 3 days, respectively. (E and F) Representative images of myotube formation in differentiated GPMs pretreated with the indicated treatments. Cells were stained with DAPI (blue) and

(legend continued on next page)

apoptosis was found to be increased in GADD45B-depleted cells at day 3 of differentiation (Figure S3E). Consistently, GADD45B deficiency significantly increased the Bcl-2-associated X protein (BAX) protein level and decreased the pro-survival protein B-cell Lymphoma-2 (BCL2) content in GPMs (Figures S3F and S3G). Taken together, these results suggest that GADD45B plays a vital role in mitochondrial biogenesis and myogenic differentiation in myoblasts.

GADD45B promotes myogenesis by activating the p38 MAPK pathway

p38 MAPK is a major regulator of skeletal muscle development and regeneration. It regulates myogenesis and mitochondria biogenesis via MRFs and PPARC1A.^{27,31} Given that GADD45B could activate the p38 MAPK pathway,³² we investigated whether the p38 MAPK pathway mediated the effect of GADD45B on myogenic differentiation and mitochondria biogenesis. First, we found that the expression of myogenic differentiation 1 (MyoD1), myogenic factor 5 (Myf5), and PPARC1A was downregulated upon depletion of GADD45B (Figure 5A). Notably, by detecting the phosphorylation levels of p38 MAPK, we found that p38 MAPK was activated during myogenic differentiation (Figure 5B). Furthermore, the formation of myotubes and the protein levels of myogenin and MyHC, which were found to be markedly repressed, were reduced in GPMs upon treatment with the p38 MAPK inhibitor SB203580 (Figures S4A–S4C). SB203580 treatment also suppressed the expression of Myf5 and PPARC1A in cells at day 1 of differentiation (Figures S4D and S4E). Taken together, these results indicate that p38 MAPK may play a crucial role in myogenic differentiation and mitochondria biogenesis.

Next, we explored whether GADD45B regulates MRFs and PPARC1A expression through the p38 MAPK pathway during myogenic differentiation. Our results showed that the phosphor-p38 MAPK level was decreased in GADD45B-depleted cells at day 1 of differentiation (Figures 5C and S5A). In contrast, GADD45B overexpression led to an increase in the level of phosphor-p38 MAPK (Figures 5D and S5B). Furthermore, MRFs (MyoD1 and Myf5) and PPARC1A were found to be dramatically downregulated in GADD45B-depleted cells (Figures 5C and S5A) but were upregulated in GADD45B-overexpressing cells (Figures 5D and S5B). These results indicate that GADD45B could affect the activity of p38 MAPK during myogenic differentiation.

To better understand the correlation among GADD45B, p38 MAPK, MRFs, and PPARC1A, the p38 MAPK inhibitor SB203580 and p38 MAPK activator hesperetin were used to block and activate p38 MAPK, respectively. Interestingly, we found that hesperetin treatment restored the decrease in myotube formation in GADD45B-depleted cells (Figures 5E and S5C), whereas SB203580 treatment dramatically antagonized the increase in myotube formation in

GADD45B-overexpressing cells (Figures 5F and S5D). In addition, hesperetin treatment also restored the expression of MRFs and PPARC1A in GADD45B-depleted cells (Figures 5G, 5I, and S5E). Similarly, SB203580 treatment also attenuated the upregulation effect of GADD45B overexpression on MRFs and PPARC1A expression (Figures 5H, 5J, and S5F). Taken together, these results suggest that GADD45B might regulate the expression of MyoD1, Myf5, and PPARC1A, as well as mediate myogenic differentiation downstream of the p38 MAPK pathway.

FTO-mediated m⁶A demethylation of GADD45B mRNA affects its stability and expression level

GADD45B was one of the upregulated genes both at the mRNA and the m⁶A modification level in kids compared to the fetuses and exhibited a positive correlation with FTO expression during myogenic differentiation (Figure 6A). Moreover, the RNA-seq dataset of FTO-knockdown GPMs was analyzed, and the results showed that GADD45B was one of 869 downregulated genes (1.5-fold change),³³ suggesting that FTO could regulate the expression of GADD45B via m⁶A modification.

To further investigate the effect of m⁶A modification on GADD45B expression, quantitative real-time PCR and western blot assays were conducted. The results showed that FTO knockdown dramatically downregulated the RNA and protein levels of GADD45B (Figures 6B–6D). The m⁶A levels were found to be upregulated in FTO-knockdown cells (Figure 6E), which could alter the mRNA instability and degradation, as well as protein translation.^{12,13} We found that the m⁶A levels in GADD45B mRNA rose from 1.5- to 3-fold in the FTO-knockdown cells, according to gene-specific m⁶A quantitative real-time PCR assays (Figure 6F). RNA stability assays³⁴ were used to measure the effect of m⁶A levels on the stability of GADD45B. A shortened half-life of GADD45B mRNA was observed in FTO-knockdown cells treated with actinomycin D compared with control cells (Figure 6G). Since GADD45B contains the RRACH m⁶A consensus motif in the 3' UTR, we constructed wild-type and mutant pmirGLO-GADD45B-3' UTR firefly luciferase reporters containing intact wild-type or mutant m⁶A sites (Figure 6H), respectively. As expected, our results showed that the luciferase activity of wild-type pmirGLO-GADD45B-3' UTR reporter, but not of mutant pmirGLO-GADD45B-3' UTR reporter, was markedly reduced upon FTO knockdown (Figure 6H). Taken together, our data demonstrate that the FTO-mediated m⁶A demethylation of GADD45B mRNA regulates its stability, thereby affecting its expression level.

FTO knockdown attenuates GADD45B-induced p38 MAPK phosphorylation and inhibits myogenic differentiation

Given the important role of FTO-mediated m⁶A in regulating myogenesis and GADD45B expression,²⁵ we investigated whether the function of FTO in myogenesis depended on GADD45B-mediated

Ab11083 (red) to image the nuclei and MyHC, respectively. Scale bars, 50 μ m. (G and H) Western blot analysis of the level of phosphorylation and non-phosphorylation of p38 MAPK, MRFs, PPARC1A, and GADD45B in differentiated GPMs pretreated with the indicated treatments. (I and J) Quantitative real-time PCR analysis of the expression of MyHC and myogenin in differentiated GPMs pretreated with the indicated treatments. The data were obtained from at least three independent experiments. The values are expressed as the mean \pm SEM; *p < 0.05, **p < 0.01.

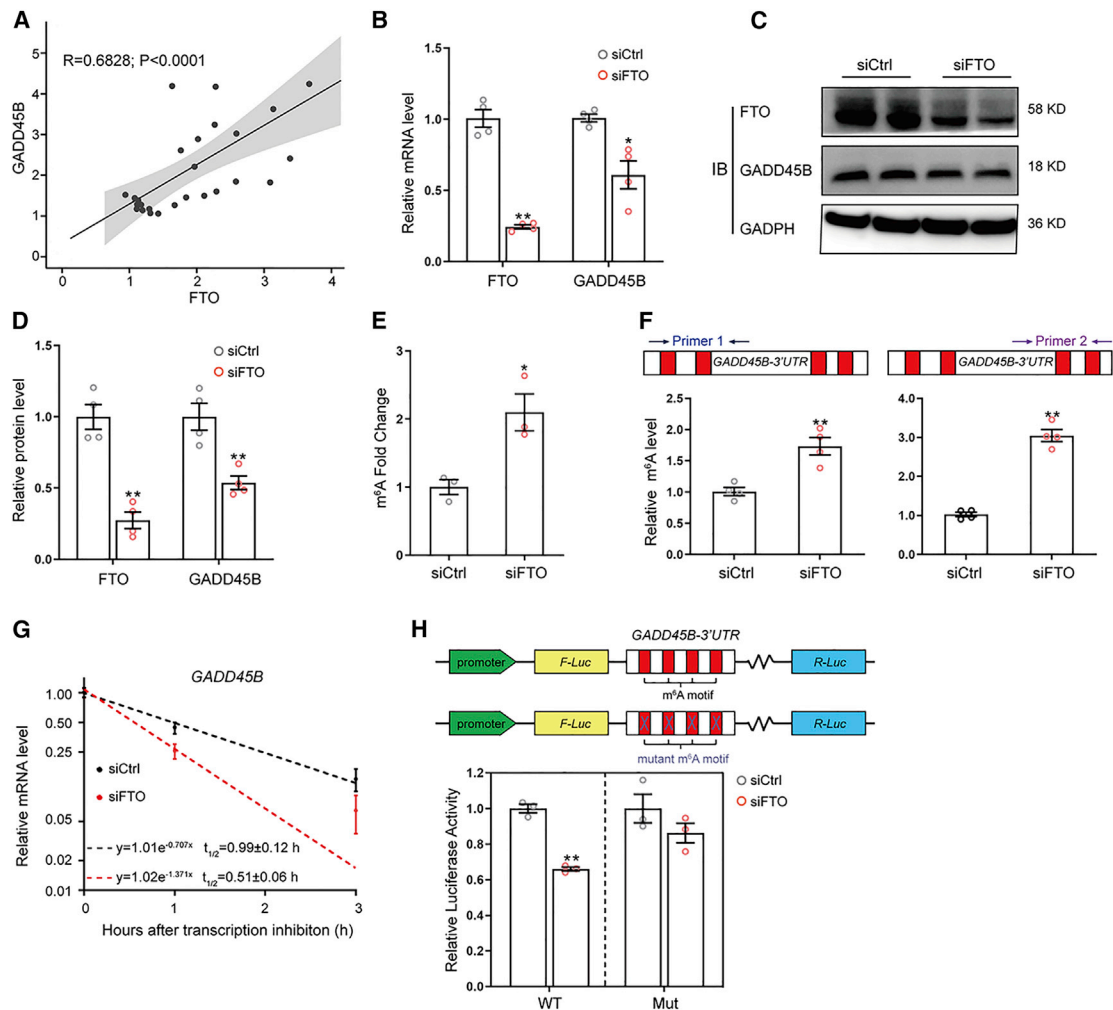


Figure 6. FTO-mediated m⁶A demethylation of GADD45B mRNA affects its stability and expression level

(A) Correlation analysis of the expression between FTO and GADD45B in GPMs at GM, D1, D2, and D3 of myogenic differentiation. The mRNA (B) and protein (C and D) expression level of GADD45B in GPMs transfected with siCtrl or FTO siRNA (siFTO), as detected using quantitative real-time PCR and western blotting. (E) The m⁶A level in GPMs transfected with siCtrl or siFTO. (F) m⁶A quantitative real-time PCR analysis of the m⁶A levels in GADD45B mRNA from GPMs transfected with siCtrl or siFTO. Two different pairs of primers were designed covering the GADD45B 3' UTR fragment containing m⁶A sites. (G) The mRNA half-life (t_{1/2}) of GADD45B in GPMs transfected with siCtrl or siFTO. (H) Relative luciferase activity of wild-type or mutant pmirGLO-GADD45B-3' UTR firefly luciferase reporter containing wild-type or mutant (A-to-T mutation) m⁶A sites, respectively, in GPMs transfected with siCtrl or siFTO. The data were obtained from at least three independent experiments. The values are expressed as the mean \pm SEM; * $p < 0.05$, ** $p < 0.01$.

p38 MAPK pathway activation. Consistent with the results of GADD45B deficiency, FTO knockdown was found to significantly decrease the phosphorylation level of p38 MAPK and subsequently suppressed the expression of MyoD1, Myf5, and PPARGC1A (Figures 7A and S6A). Moreover, the expression of MyHC and myogenin was reduced, and myotube formation was attenuated upon FTO knockdown (Figures 7B, 7C, 7D, and S6B). Notably, in FTO-silenced cells, mitochondria biogenesis and the related gene expression were suppressed (Figures S7A–S7G), along with a decrease in ATP production (Figure S7H), similar to the results of GADD45B deficiency. Interestingly, the forced expression of GADD45B CDS alone rescued the inhibition of GADD45B expression caused by FTO knockdown

(Figures 7E, 7F, and S6C), subsequently improving myotube formation in FTO-depleted cells (Figure 7G). Furthermore, GADD45B overexpression restored the reduced phosphorylation levels of p38 MAPK and the PPARGC1A, MyoD1, Myf5, myogenin, and MyHC expression levels in FTO-depleted cells (Figures 7H, 7I, and S6D). Consistently, hesperetin treatment achieved a similar restoration effect regarding myotube formation, phosphorylation levels of p38 MAPK, and MRFs and PPARGC1A expression levels (Figures S8A–S8C), as observed upon GADD45B overexpression in FTO-depleted conditions. Taken together, our findings indicate that FTO regulates myogenic differentiation via the GADD45B-p38 MAPK pathway.

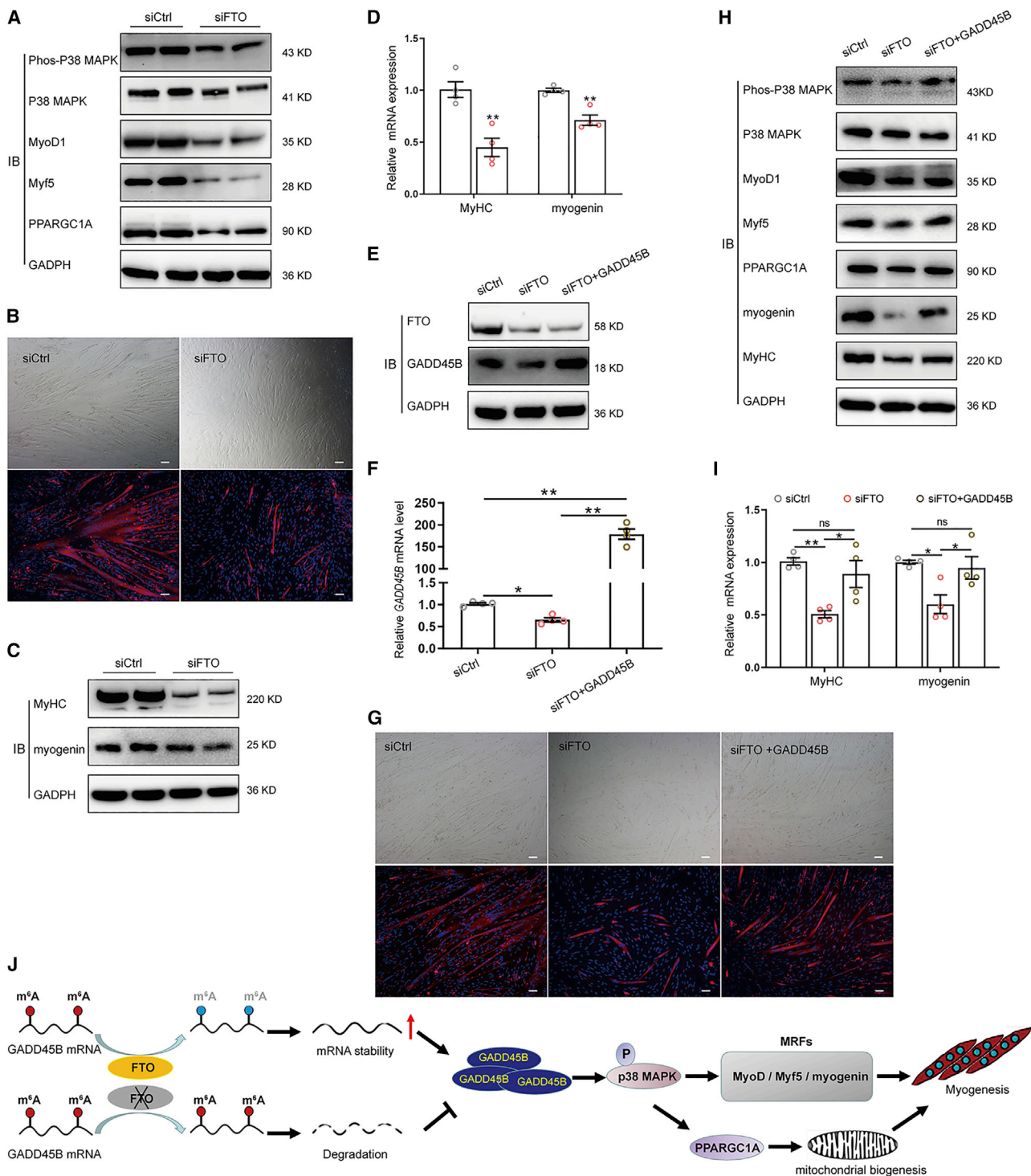


Figure 7. FTO-mediated downregulation of GADD45B suppresses myogenic differentiation

(A) Western blot analysis of the level of phosphorylation and non-phosphorylation of p38 MAPK, MyoD1, Myf5, and PPARGC1A in siCtrl and siFTO cells at D1 of differentiation. (B) Representative images of myotube formation in siCtrl and siFTO cells at D3 of differentiation. Cells were stained with DAPI (blue) and Ab11083 (red) to image the nuclei and MyHC, respectively. Scale bars, 50 μ m. The protein (C) and mRNA (D) expression levels of MyHC and myogenin in siCtrl and siFTO cells at day 3 of differentiation were detected using western blot and quantitative real-time PCR, respectively. The protein (E) and mRNA (F) expression levels of GADD45B in GPMs transfected with siCtrl, siFTO, and siFTO + pEX3-GADD45B plasmid (siFTO + GADD45B), as detected using western blotting and quantitative real-time PCR. (G) Representative images of myotube (legend continued on next page)

DISCUSSION

In the present study, we mapped the pattern of global m⁶A modifications in goat skeletal muscle during embryonic development and demonstrated that GADD45B, which is regulated by m⁶A modification, is an important regulator of myogenesis. GADD45B deficiency was found to decrease the phosphorylation levels of p38 MAPK, thereby downregulating the expression of MRFs and PPARGC1A, leading to the suppression of myogenic differentiation and mitochondria biogenesis. The knockdown of FTO was found to increase the level of m⁶A modification in GADD45B, which in turn accelerated the degradation of its mRNA and downregulated its transcription and protein levels. The knockdown of FTO significantly impaired myogenic differentiation, which was found to be restored by GADD45B overexpression. These results indicate that the FTO-mediated m⁶A modification of GADD45B mRNA plays a critical role in muscle differentiation.

The transcriptional regulatory networks that control the specification of muscle precursor cells and the expression of myogenic regulatory genes have been well defined in mammals. However, the role of post-transcriptional modifications in skeletal muscle development is only just being gradually discovered. m⁶A modifications represent a new type of post-transcriptional gene regulation and play a vital role in the development of a variety of tissues, including cerebellar development,³⁵ oocyte development,³⁶ and adipogenesis.³⁷ Interestingly, a reduction in the lean body mass was commonly observed in FTO knockout mice,^{24,38} caused by the dysregulation of energy expenditure induced by disorders of FTO expression. Notably, the deficiency in the demethylase activity of FTO was a major factor leading to the impairment of muscle differentiation and skeletal muscle development.²⁵ In our study, the m⁶A level was decreased during myogenic differentiation *in vivo* and *in vitro*. Thus, it is likely that m⁶A modifications may be involved in the regulation of skeletal muscle development. However, the genes that are modified by m⁶A to regulate skeletal muscle development remain unknown.

GADD45B, also known as Myd118, is a member of the GADD45 gene family, which is involved in the process of response to cell injury caused by physiological or environmental stressors.³⁹ GADD45B is highly expressed in the chorion during embryonic development⁴⁰ and has been reported to play a vital role in brain development, including in neurogenesis⁴¹ and in dendritic development.⁴² Although there is still a lack of evidence showing that GADD45B directly controls muscle development, it has been demonstrated that GADD45B could regulate the downstream p38 MAPK signaling pathway, which is associated with myogenesis.^{32,43} In our study, GADD45B was identified as a m⁶A-modified gene and was found to be upregulated during myogenic differentiation. Furthermore,

GADD45B knockdown was found to impair myogenic differentiation and mitochondria biogenesis in myoblasts, whereas the forced expression of GADD45B promoted myogenic differentiation. Future studies will be needed to confirm the potential roles of GADD45B in skeletal muscle development *in vivo* using GADD45B knockout mice.

Next, we elucidated the mechanism underlying the role of GADD45B in myogenic differentiation and found that GADD45B expression influenced the activity of p38 MAPK during myogenic differentiation. p38 MAPK, a subgroup of the MAPK superfamily of intracellular serine/threonine protein kinases, is known to regulate the differentiation of various cell types, such as adipocytes and muscle stem cells. It also regulates the expression of MRFs, including Myf5, MyoD1, myogenin, and MRF4.^{44,45} Interestingly, GADD45B can also regulate the expression of MyoD1, Myf5, and myogenin genes. However, when p38 MAPK activity was blocked by SB203580 treatment, the effect of GADD45B on the transcription of MRFs was attenuated, suggesting that the GADD45B-mediated regulation of MRFs depends on p38 MAPK activity. During the differentiation of skeletal myoblasts into myotubes, a cellular metabolic-style shift from glycolysis to oxidative phosphorylation occurs.⁴⁶ To adapt to this change, the complex mitochondrial network is remodeled through mitochondrial clearance and biogenesis during myogenic differentiation.²⁸ Therefore, maintaining the balance of mitochondrial clearance and biogenesis is indispensable for myogenesis. PPARGC1A, also known as peroxisome proliferator-activated receptor gamma coactivator 1 alpha (PGC-1 α), is a master regulator of mitochondrial biogenesis, modulating the transcription of nuclear genes encoding mitochondrial proteins.⁴⁷ It has been demonstrated that PPARGC1A sustains mitochondrial homeostasis during myogenesis by blocking excessive ROS production, which can result in the degradation of the mitochondrial network via mitophagy.⁴⁸ In line with these findings, GADD45B knockdown downregulates PPARGC1A, resulting in an increased ROS production, autophagy, and apoptosis, leading to a decrease in the mitochondrial content. Furthermore, our results show that the ability of GADD45B to regulate PPARGC1A expression relies on p38 MAPK activity, which is in agreement with the results of a previous study that found that the p38 MAPK pathway affects PPARGC1A expression.⁴⁹ Taken together, the results presented in this study indicate that GADD45B regulates myogenic differentiation via the p38 MAPK-MRFs and p38 MAPK-PPARGC1A-mitochondria axes, demonstrating that the p38 MAPK activation is essential for the GADD45B-mediated myogenic differentiation.

It is well known that the expression of the genes of the GADD45 family is induced by various endogenous and exogenous stress stimuli. To accurately respond to complex cellular stress stimuli, the stress sensors on GADD45 proteins need to be rapidly regulated at both

formation in siCtrl, siFTO, and siFTO + GADD45B cells at day 3 of differentiation. Scale bars, 50 μ m. (H) Western blot analysis of phosphorylation and non-phosphorylation of p38 MAPK, MRFs, and PPARGC1A in siCtrl, siFTO, and siFTO + GADD45B cells at day 3 of differentiation. (I) Quantitative real-time PCR analysis of *MyHC* and *myogenin* in siCtrl, siFTO, and siFTO + GADD45B cells at day 3 of differentiation. (J) Graphical representation of the role and underlying mechanism of the FTO-mediated demethylation of GADD45B in myogenesis. The data were obtained from at least three independent experiments. The values are expressed as the mean \pm SEM; *p < 0.05, **p < 0.01.

the transcriptional and post-transcriptional levels.³⁹ Under different stress induction signals, GADD45B is distinctly regulated at the mRNA transcription or mRNA stability level.⁵⁰ However, little is known about whether GADD45B is subject to m⁶A modifications. In the current study, we found that the knockdown of FTO leads to an increase in the m⁶A levels in the 3' UTR of GADD45B, which decreased the mRNA stability and reduced GADD45B expression. To our knowledge, this study is the first to demonstrate that post-transcriptional m⁶A modifications are involved in the regulation of the GADD45B mRNA levels during myogenic differentiation. Although FTO has been reported to regulate myogenic differentiation via the mechanistic target of rapamycin kinase (mTOR) pathway,²⁵ the specific genes subject to FTO-mediated m⁶A modifications in this process have not yet been identified. However, our results indicate that FTO demethylates GADD45B mRNA and regulates myogenic differentiation via the p38 MAPK pathway. It is worth noting that other genes carrying an m⁶A modification could be targeted by FTO and be involved in myogenic differentiation, in addition to GADD45B. More studies will be needed to investigate and identify additional genes in order to clarify the function of m⁶A modifications during skeletal muscle differentiation.

In conclusion, our results demonstrate that GADD45B promotes myogenic differentiation by activating the p38 MAPK pathway and is regulated by FTO-mediated m⁶A modifications (Figure 7). These findings highlight the importance of the m⁶A modification-mediated regulation of gene expression during myogenic differentiation and provide new insights into the molecular mechanisms underlying skeletal muscle development.

MATERIALS AND METHODS

Animal samples

All animal studies were performed under the guidelines of the Ethics Committee of Nanjing Agricultural University, China. All goats used in this study were from Haimen goat breeding farm, in Nantong, China. Sixteen female goats in good body condition and suitable for pregnancy were selected. All selected goats underwent estrus synchronization treatment and were naturally mated. After 75 days of gestation, four male fetuses were removed from five pregnant goats during abortion operations, and their longissimus muscle samples were collected. After natural parturition of other pregnant goats, four male goats were selected from the newborn goats, and they were sacrificed via exsanguination for longissimus muscle sampling.

Histological analysis

The longissimus muscle samples from goats were collected and preserved in 4% paraformaldehyde overnight at room temperature before paraffin embedding. The H&E-stained cross-sections of the longissimus muscles from each animal were imaged using a microscope (Nikon, Tokyo, Japan). The fibers (2,500 μm^2) in five fields were counted from each animal (n = 4) using ImageJ software (National Institutes of Health, Bethesda, MD, USA). In addition, the cross-section area of each fiber (n > 1,000) in the five fields

(n = 4) was determined using ImageJ (National Institutes of Health, Bethesda, MD, USA).

Cell culture

GPMs collected from goat fetuses at the embryonic stage (75 days) were cultured as previously described.⁵¹ Briefly, the hindlimb muscle tissues were minced into pieces and digested with 1% collagenase I (Sigma-Aldrich) for 50 min at 37°C with slight agitation and then digested with 0.25% trypsin (Gibco) for 15 min at 37°C. The digested samples were filtered through a 70- μm filter and then centrifuged to collect the cells. Cells were plated in growth media (DMEM containing 20% fetal bovine serum (FBS), 10% horse serum, and 1% penicillin/streptomycin). After 2 h, the non-adherent cells were transferred to another culture dish. To obtain pure GPMs, the differential adhesion method was performed as previously described.⁵¹

GPMs were cultured at 37°C and 5% CO₂ in growth media. To induce differentiation, GPMs were grown to about 80% confluence in growth media and then switched to differentiation medium (DMEM containing 2% horse serum and 1% penicillin/streptomycin).

Cell transfection

siRNAs and plasmids were transfected into cells using Lipofectamine 3000 transfection reagent (Life Technologies) and LIPOFECTAMINE LTX transfection reagent (Life Technologies), respectively, according to the manufacturer's instructions. All siRNA sequences were designed and synthesized by Genepharma (Shanghai, China), as listed in Table S4. The GADD45B CDS was amplified from the *Capra hircus* GADD45B gene (XM_018050778.1) using PCR by using primers GADD45B-NotI-5.1 and GADD45B-EcoRI-3.1 and then cloned into a pEX3 vector (Genepharma) to generate the pEX3-GADD45B plasmid. The primers used for cloning GADD45B CDS are listed in Table S5.

RNA extraction and quantitative real-time PCR

Trizol reagent (Invitrogen) was used to extract the total RNA from the tissues or cells. The extracted RNA was then reverse transcribed into cDNA using reverse transcription reagent kits (Takara, Dalian, China), according to the manufacturer's instructions. Quantitative real-time PCR analysis was performed using the SYBR Green PCR Master Mix (Roche) and the QuantStudio 5 Real-Time PCR System (Applied Biosystems, Bedford, MA, USA). The relative gene expression was quantified using the 2^{- $\Delta\Delta\text{Ct}$} method by using 18S rRNA as an endogenous control. The primers used are listed in Table S5.

Quantification of m⁶A modifications

The extracted RNA was purified using GenElute mRNA Miniprep (MRN10; Sigma-Aldrich). After analyzing the quality of the purified RNA using NanoDrop, the global m⁶A RNA methylation was measured using an EpiQuik m⁶A RNA Methylation Quantification Kit (P-9005-48; Epigentek), following the manufacturer's protocol. The global m⁶A levels were measured colorimetrically by reading the absorbance at 450 nm and calculated using the resulting standard curve.

m⁶A-seq assays

For m⁶A-seq, 200 µg of total RNA was subjected to poly(A) mRNA isolation using poly-T oligo-attached magnetic beads (Invitrogen). Following purification, the poly(A) mRNA fractions were fragmented using divalent cations at high temperatures. Then, random RNA fragments (~100 nucleotides) were incubated with an m⁶A-specific antibody (number [no.] 202003; Synaptic Systems) in immunoprecipitation (IP) buffer (10 mM Tris-HCl, 150 mM NaCl, and 0.1% Igepal CA-630) for 2 h at 4°C. The mixture was then incubated with protein-A beads and eluted using elution buffer (1 × IP buffer and 6.7 mM m⁶A). The eluted RNA was precipitated using 75% ethanol. Eluted m⁶A-containing fragments (IP) and untreated input control fragments were used to obtain the final cDNA library in accordance with a strand-specific library preparation by using the deoxynucleotide triphosphate (dUTP) method. The resulting library was subjected to paired-end 2 × 150 bp sequencing using an Illumina NovaSeq 6000 platform at LC-BIO Bio-Tech (Hangzhou, China).

Immunofluorescence and confocal imaging

Cells were fixed in 4% paraformaldehyde and washed with PBS. The samples were permeabilized in 0.25% Triton X-100 and incubated with 3% bovine serum albumin for 1 h at room temperature, followed by incubation with a diluted solution of the following antibodies: anti-PAX7, anti-Desmin, anti-Myf5, or anti-MyHC, at 4°C overnight. After washing with PBS, the cells were incubated with the secondary antibody for 1 h at room temperature. The cell nuclei were then colored with 4',6'-diamidino-2-phenylindole (DAPI), and the fluorescence images were analyzed using a fluorescence microscope (Jena).

Immunoblotting

Cells were lysed in radioimmunoprecipitation assay (RIPA) buffer (Thermo Fisher Scientific) containing a cocktail of protease inhibitors. Approximately 20 µg of extracted protein was loaded and separated on 8% ~12% SDS-PAGE gels, transferred to polyvinylidene fluoride (PVDF) membranes (Millipore, MA, USA), and blocked for 1 h at room temperature with 5% skim milk. After washing with Tris-buffered saline containing Tween-20 (TBST), the membranes were incubated overnight with the corresponding primary antibodies at 4°C. Then, the membranes were washed with TBST and incubated with the appropriate horseradish peroxidase secondary antibodies at room temperature for 1 h. The bands were visualized using ECL Plus Western Blotting Reagent Pack (Bio-Rad). The primary antibodies used are listed in [Table S6](#).

Transmission electron microscopy

The cells were harvested from the cell culture dishes using trypsin and centrifuged for 7 min at 350 × g. After washing with PBS, the cells were fixed in a glutaric dialdehyde solution (Solarbio) for 20 min. Then, the cells were post-fixed in 1% OsO₄ in 0.1 M phosphate buffer (PB; pH 7.4) for 2 h on a rotator. Subsequently, the cells were dehydrated using an ethanol-graded series and infiltrated using a Spurr's resin-graded series. After polymerization, the resin blocks were cut into 60–80 nm-thick sections using an ultramicrotome (Leica Micro-

systems, Wetzlar, Germany). The sections were fished out onto 150 mesh cuprum grids using formvar film (G300-Cu; Electron Microscopy Sciences). The sections were stained with a 2% uranium acetate saturated alcohol solution and 2.6% lead citrate and examined using a transmission electron microscope (FEI, Hillsboro, OR, USA).

Mitochondrial content assay

Mitochondrial content assays were performed according to the protocol described by Iwabu et al.⁵² The mitochondrial content was evaluated using mtDNA quantification and Mito-tracker staining. The mtDNA copy number was measured using quantitative real-time PCR by quantifying the ratio of the mitochondrial *Cox2* gene to an endogenous gene of the nuclear 18S rRNA. The primer sequences used are listed in [Table S5](#).

Cells were incubated with 100 nM Mito-tracker Green (Beyotime Biotechnology) for 30 min at 37°C. After washing with PBS, cells were collected via trypsin/EDTA digestion and resuspended in PBS. Fluorescence intensity was measured using excitation and emission wavelengths of 490 and 516 nm, respectively, and the values were corrected for total protein (micrograms per milliliter).

ATP measurement

The intracellular ATP content was measured using an ATP assay kit (Beyotime) following the manufacturer's protocol.

Intracellular ROS measurement

Cells were incubated with 50 µM dichlorofluorescein diacetate (DCF-DA; Beyotime Biotechnology) for 30 min at 37°C and then were washed with PBS. Immunofluorescence was observed using a fluorescence microscope (Leica, Germany). The fluorescence intensity of the images was analyzed using ImageJ software.

Flow cytometry

Cells were harvested and washed in PBS before being resuspended in annexin A5 (ANXA5) binding buffer and incubated with 5 µL of ANXA5-fluorescein isothiocyanate (FITC; Thermo Fisher Scientific) and 10 µL of propidium iodide (PI) (50 µg/mL; Sigma-Aldrich). The cells were then analyzed using a flow cytometer (BD FACSCalibur).

m⁶A quantitative real-time PCR

The RNA IP (RIP) procedure was performed as previously described.⁵³ Briefly, the total RNA was obtained from cells using TRIzol and then purified using GenElute mRNA Miniprep (MRN10; Sigma-Aldrich). Poly(A) RNA was fragmented using an RNA fragmentation reagent and immunoprecipitated using m⁶A antibody for m⁶A IP. Finally, the m⁶A-bound fraction RNA was recovered via ethanol precipitation, and the m⁶A enrichment was determined using quantitative real-time PCR analysis.

RNA stability assays

The cells were transfected with either control siRNA (siCtrl) or FTO siRNA (siFTO) for 24 h and then treated with 5 µg/mL actinomycin D (HY-17559; MedChemExpress [MCE]) for 0, 1, or 3 h to inhibit

global mRNA transcription, after which, the samples were collected to assess their degradation. The RNA was extracted using TRIzol reagent and then reverse transcribed, as previously described. The mRNA transcript levels were detected by using quantitative real-time PCR. The degradation rate of the RNA was estimated as previously described.^{13,54}

Dual-luciferase reporter and mutagenesis assays

The DNA fragments of GADD45B-3' UTR containing the wild-type m⁶A and mutant motifs (m⁶A was replaced by T) were directly synthesized by Genepharma (Shanghai, China). The GADD45B-3' UTR sequences used are listed in Table S7. Wild-type and mutant GADD45B-3' UTR were then inserted into pmirGLO vector (Promega) between the SacI and XhoI enzyme sites. For the dual-luciferase reporter assay, 200 ng of wild-type or mutant pmirGLO-GADD45B-3' UTR and siFTO were co-transfected into GPMs in 24-well plates. After 48 h of transfection, the relative luciferase activity was measured using a dual-luciferase reporter assay system (Vazyme).

Statistical analysis

All experiments were carried out at least in triplicates. All data are expressed as the mean \pm SEM. Statistical analysis was performed using SPSS software (version 24.0; SPSS, Chicago, IL, USA) using a two-tailed Student's t test or one-way analysis of variance (ANOVA) followed by Tukey's post hoc analysis. For all the analyses, $p < 0.05$ was considered significant.

SUPPLEMENTAL INFORMATION

Supplemental information can be found online at <https://doi.org/10.1016/j.omtn.2021.06.013>.

ACKNOWLEDGMENTS

We thank Dr. Zhaoyu Sun, Jingang Wang, and Master Haifeng Zhang for their help in sampling; Prof. Xiangpeng Dai, Dr. Zhifei Liu, Jian Zheng, and Xiaodan Li for their general assistance; and the High-Performance Computing Platform of Bioinformatics Center, Nanjing Agricultural University, for its support in data analysis. This research was supported by the National Key R&D program of China (2018YFD0501900, 901) and the Key Project for JiangSu Agricultural New Variety Innovation (PZCZ201740).

AUTHOR CONTRIBUTIONS

K.D. and F.W. conceived and designed the study. K.D., Y.L., and Y.C. performed the experiments. K.D., Y.F., and M.D. analyzed the data. Z.W., J.L., and J.S. performed tissue sampling. K.D. wrote and revised the manuscript. F.W. and Y.Z. supervised the study and administered the project.

DECLARATION OF INTERESTS

The authors declare no competing interests.

REFERENCES

- Lehka, L., and Redowicz, M.J. (2020). Mechanisms regulating myoblast fusion: A multilevel interplay. *Semin. Cell Dev. Biol.* *104*, 81–92.
- Yin, H., Price, F., and Rudnicki, M.A. (2013). Satellite cells and the muscle stem cell niche. *Physiol. Rev.* *93*, 23–67.
- Potthoff, M.J., and Olson, E.N. (2007). MEF2: a central regulator of diverse developmental programs. *Development* *134*, 4131–4140.
- Cisternas, P., Henriquez, J.P., Brandan, E., and Inestrosa, N.C. (2014). Wnt signaling in skeletal muscle dynamics: myogenesis, neuromuscular synapse and fibrosis. *Mol. Neurobiol.* *49*, 574–589.
- Blais, A., Tsikitis, M., Acosta-Alvear, D., Sharan, R., Kluger, Y., and Dynlacht, B.D. (2005). An initial blueprint for myogenic differentiation. *Genes Dev.* *19*, 553–569.
- Hagan, M., Zhou, M., Ashraf, M., Kim, L.M., Su, H., Weintraub, N.L., and Tang, Y. (2017). Long noncoding RNAs and their roles in skeletal muscle fate determination. *Non-coding RNA Investig.* *1*, 24.
- Das, A., Das, A., Das, D., Abdelmohsen, K., and Panda, A.C. (2020). Circular RNAs in myogenesis. *Biochim. Biophys. Acta. Gene Regul. Mech.* *1863*, 194372.
- Apponi, L.H., Corbett, A.H., and Pavlath, G.K. (2011). RNA-binding proteins and gene regulation in myogenesis. *Trends Pharmacol. Sci.* *32*, 652–658.
- Roundtree, I.A., Evans, M.E., Pan, T., and He, C. (2017). Dynamic RNA Modifications in Gene Expression Regulation. *Cell* *169*, 1187–1200.
- Boccalletto, P., Machnicka, M.A., Purta, E., Piatkowski, P., Baginski, B., Wirecki, T.K., de Crécy-Lagard, V., Ross, R., Limbach, P.A., Kötter, A., et al. (2018). MODOMICS: a database of RNA modification pathways. 2017 update. *Nucleic Acids Res.* *46* (D1), D303–D307.
- Dominissini, D., Moshitch-Moshkovitz, S., Schwartz, S., Salmon-Divon, M., Ungar, L., Osenberg, S., Cesarkas, K., Jacob-Hirsch, J., Amariglio, N., Kupiec, M., et al. (2012). Topology of the human and mouse m⁶A RNA methylomes revealed by m⁶A-seq. *Nature* *485*, 201–206.
- Wang, X., Zhao, B.S., Roundtree, I.A., Lu, Z., Han, D., Ma, H., Weng, X., Chen, K., Shi, H., and He, C. (2015). N(6)-methyladenosine Modulates Messenger RNA Translation Efficiency. *Cell* *161*, 1388–1399.
- Wang, X., Lu, Z., Gomez, A., Hon, G.C., Yue, Y., Han, D., Fu, Y., Parisien, M., Dai, Q., Jia, G., et al. (2014). N6-methyladenosine-dependent regulation of messenger RNA stability. *Nature* *505*, 117–120.
- Wang, X., Feng, J., Xue, Y., Guan, Z., Zhang, D., Liu, Z., Gong, Z., Wang, Q., Huang, J., Tang, C., et al. (2017). Corrigendum: Structural basis of N⁶-adenosine methylation by the METTL3-METTL14 complex. *Nature* *542*, 260.
- Ping, X.-L., Sun, B.-F., Wang, L., Xiao, W., Yang, X., Wang, W.-J., Adhikari, S., Shi, Y., Lv, Y., Chen, Y.-S., et al. (2014). Mammalian WTAP is a regulatory subunit of the RNA N6-methyladenosine methyltransferase. *Cell Res.* *24*, 177–189.
- Meyer, K.D., and Jaffrey, S.R. (2017). Rethinking m⁶A Readers, Writers, and Erasers. *Annu. Rev. Cell Dev. Biol.* *33*, 319–342.
- Chen, T., Hao, Y.-J., Zhang, Y., Li, M.-M., Wang, M., Han, W., Wu, Y., Lv, Y., Hao, J., Wang, L., et al. (2015). m(6)A RNA methylation is regulated by microRNAs and promotes reprogramming to pluripotency. *Cell Stem Cell* *16*, 289–301.
- Guo, M., Liu, X., Zheng, X., Huang, Y., and Chen, X. (2017). m⁶A RNA Modification Determines Cell Fate by Regulating mRNA Degradation. *Cell. Reprogram.* *19*, 225–231.
- Engel, M., Eggert, C., Kaplick, P.M., Eder, M., Röh, S., Tietze, L., Namendorf, C., Arloth, J., Weber, P., Rex-Haffner, M., et al. (2018). The Role of m⁶A/m-RNA Methylation in Stress Response Regulation. *Neuron* *99*, 389–403.e9.
- Fitzsimmons, C.M., and Batista, P.J. (2019). It's complicated... m⁶A-dependent regulation of gene expression in cancer. *Biochim. Biophys. Acta. Gene Regul. Mech.* *1862*, 382–393.
- Wang, Y., Gao, M., Zhu, F., Li, X., Yang, Y., Yan, Q., Jia, L., Xie, L., and Chen, Z. (2020). METTL3 is essential for postnatal development of brown adipose tissue and energy expenditure in mice. *Nat. Commun.* *11*, 1648.
- Wu, Y., Xie, L., Wang, M., Xiong, Q., Guo, Y., Liang, Y., Li, J., Sheng, R., Deng, P., Wang, Y., et al. (2018). Mettl3-mediated m⁶A RNA methylation regulates the fate of bone marrow mesenchymal stem cells and osteoporosis. *Nat. Commun.* *9*, 4772.
- Yoon, K.J., Ringeling, F.R., Vissers, C., Jacob, F., Pokrass, M., Jimenez-Cyrus, D., Su, Y., Kim, N.S., Zhu, Y., Zheng, L., et al. (2017). Temporal Control of Mammalian Cortical Neurogenesis by m⁶A Methylation. *Cell* *171*, 877–889.e17.

24. McMurray, F., Church, C.D., Larder, R., Nicholson, G., Wells, S., Teboul, L., Tung, Y.C., Rimmington, D., Bosch, F., Jimenez, V., et al. (2013). Adult onset global loss of the *fto* gene alters body composition and metabolism in the mouse. *PLoS Genet.* *9*, e1003166.
25. Wang, X., Huang, N., Yang, M., Wei, D., Tai, H., Han, X., Gong, H., Zhou, J., Qin, J., Wei, X., et al. (2017). FTO is required for myogenesis by positively regulating mTOR-PGC-1 α pathway-mediated mitochondria biogenesis. *Cell Death Dis.* *8*, e2702.
26. Chen, S., Li, Y., Zhi, S., Ding, Z., Wang, W., Peng, Y., Huang, Y., Zheng, R., Yu, H., Wang, J., et al. (2020). WTAP promotes osteosarcoma tumorigenesis by repressing HMBOX1 expression in an m⁶A-dependent manner. *Cell Death Dis.* *11*, 659.
27. Segalés, J., Perdiguero, E., and Muñoz-Cánoves, P. (2016). Regulation of Muscle Stem Cell Functions: A Focus on the p38 MAPK Signaling Pathway. *Front. Cell Dev. Biol.* *4*, 91.
28. Sin, J., Andres, A.M., Taylor, D.J.R., Weston, T., Hiraumi, Y., Stotland, A., Kim, B.J., Huang, C., Doran, K.S., and Gottlieb, R.A. (2016). Mitophagy is required for mitochondrial biogenesis and myogenic differentiation of C2C12 myoblasts. *Autophagy* *12*, 369–380.
29. Remels, A.H., Langen, R.C., Schrauwen, P., Schaart, G., Schols, A.M., and Gosker, H.R. (2010). Regulation of mitochondrial biogenesis during myogenesis. *Mol. Cell. Endocrinol.* *315*, 113–120.
30. You, W., Xu, Z., Sun, Y., Valencak, T.G., Wang, Y., and Shan, T. (2020). GADD45 α drives brown adipose tissue formation through upregulating PPAR γ in mice. *Cell Death Dis.* *11*, 585.
31. Gibala, M.J., McGee, S.L., Garnham, A.P., Howlett, K.F., Snow, R.J., and Hargreaves, M. (2009). Brief intense interval exercise activates AMPK and p38 MAPK signaling and increases the expression of PGC-1 α in human skeletal muscle. *J. Appl. Physiol.* (1985) *106*, 929–934.
32. Keil, E., Höcker, R., Schuster, M., Essmann, F., Ueffing, N., Hoffman, B., Liebermann, D.A., Pfeffer, K., Schulze-Osthoff, K., and Schmitz, I. (2013). Phosphorylation of Atg5 by the Gadd45 β -MEKK4-p38 pathway inhibits autophagy. *Cell Death Differ.* *20*, 321–332.
33. Deng, K., Zhang, Z., Ren, C., Liang, Y., Gao, X., Fan, Y., and Wang, F. (2021). FTO regulates myoblast proliferation by controlling CCND1 expression in an m⁶A-YTHDF2-dependent manner. *Exp. Cell Res.* *401*, 112524.
34. Hu, X., Peng, W.X., Zhou, H., Jiang, J., Zhou, X., Huang, D., Mo, Y.Y., and Yang, L. (2020). IGF2BP2 regulates DANCR by serving as an N6-methyladenosine reader. *Cell Death Differ.* *27*, 1782–1794.
35. Wang, C.X., Cui, G.S., Liu, X., Xu, K., Wang, M., Zhang, X.X., Jiang, L.Y., Li, A., Yang, Y., Lai, W.Y., et al. (2018). METTL3-mediated m6A modification is required for cerebellar development. *PLoS Biol.* *16*, e2004880.
36. Kasowitz, S.D., Ma, J., Anderson, S.J., Leu, N.A., Xu, Y., Gregory, B.D., Schultz, R.M., and Wang, P.J. (2018). Nuclear m6A reader YTHDC1 regulates alternative polyadenylation and splicing during mouse oocyte development. *PLoS Genet.* *14*, e1007412.
37. Wang, X., Wu, R., Liu, Y., Zhao, Y., Bi, Z., Yao, Y., Liu, Q., Shi, H., Wang, F., and Wang, Y. (2020). m⁶A mRNA methylation controls autophagy and adipogenesis by targeting *Atg5* and *Atg7*. *Autophagy* *16*, 1221–1235.
38. Speakman, J.R. (2010). FTO effect on energy demand versus food intake. *Nature* *464*, E1–discussion, E2.
39. Salvador, J.M., Brown-Clay, J.D., and Fornace, A.J., Jr. (2013). Gadd45 in stress signaling, cell cycle control, and apoptosis. *Adv. Exp. Med. Biol.* *793*, 1–19.
40. Kaufmann, L.T., Gierl, M.S., and Niehrs, C. (2011). Gadd45a, Gadd45b and Gadd45g expression during mouse embryonic development. *Gene Expr. Patterns* *11*, 465–470.
41. Ma, D.K., Jang, M.H., Guo, J.U., Kitabatake, Y., Chang, M.L., Pow-Anpongkul, N., Flavell, R.A., Lu, B., Ming, G.L., and Song, H. (2009). Neuronal activity-induced Gadd45b promotes epigenetic DNA demethylation and adult neurogenesis. *Science* *323*, 1074–1077.
42. Sultan, F.A., Wang, J., Tront, J., Liebermann, D.A., and Sweatt, J.D. (2012). Genetic deletion of Gadd45b, a regulator of active DNA demethylation, enhances long-term memory and synaptic plasticity. *J. Neurosci.* *32*, 17059–17066.
43. Chen, Z., Wan, X., Hou, Q., Shi, S., Wang, L., Chen, P., Zhu, X., Zeng, C., Qin, W., Zhou, W., and Liu, Z. (2016). GADD45B mediates podocyte injury in zebrafish by activating the ROS-GADD45B-p38 pathway. *Cell Death Dis.* *7*, e2068.
44. Simone, C., Forcales, S.V., Hill, D.A., Imbalzano, A.N., Latella, L., and Puri, P.L. (2004). p38 pathway targets SWI-SNF chromatin-remodeling complex to muscle-specific loci. *Nat. Genet.* *36*, 738–743.
45. Lluís, F., Perdiguero, E., Nebreda, A.R., and Muñoz-Cánoves, P. (2006). Regulation of skeletal muscle gene expression by p38 MAP kinases. *Trends Cell Biol.* *16*, 36–44.
46. Wagatsuma, A., and Sakuma, K. (2013). Mitochondria as a potential regulator of myogenesis. *ScientificWorldJournal* *2013*, 593267.
47. Aquilano, K., Vigilanza, P., Baldelli, S., Pagliei, B., Rotilio, G., and Ciriolo, M.R. (2010). Peroxisome proliferator-activated receptor gamma co-activator 1 α (PGC-1 α) and sirtuin 1 (SIRT1) reside in mitochondria: possible direct function in mitochondrial biogenesis. *J. Biol. Chem.* *285*, 21590–21599.
48. Baldelli, S., Aquilano, K., and Ciriolo, M.R. (2014). PGC-1 α buffers ROS-mediated removal of mitochondria during myogenesis. *Cell Death Dis.* *5*, e1515.
49. Akimoto, T., Pohnert, S.C., Li, P., Zhang, M., and Gumbs, C. (2005). Exercise stimulates PGC-1 α transcription in skeletal muscle through activation of the p38 MAPK pathway. *J. Biol. Chem.* *280*, 19587–19593.
50. Zumbun, S.D., Hoffman, B., and Liebermann, D.A. (2009). Distinct mechanisms are utilized to induce stress sensor gadd45b by different stress stimuli. *J. Cell. Biochem.* *108*, 1220–1231.
51. Gharaibeh, B., Lu, A., Tebbets, J., Zheng, B., Feduska, J., Crisan, M., Péault, B., Cummins, J., and Huard, J. (2008). Isolation of a slowly adhering cell fraction containing stem cells from murine skeletal muscle by the preplate technique. *Nat. Protoc.* *3*, 1501–1509.
52. Iwabu, M., Yamauchi, T., Okada-Iwabu, M., Sato, K., Nakagawa, T., Funata, M., Yamaguchi, M., Namiki, S., Nakayama, R., Tabata, M., et al. (2010). Adiponectin and AdipoR1 regulate PGC-1 α and mitochondria by Ca(2+) and AMPK/SIRT1. *Nature* *464*, 1313–1319.
53. Dominissini, D., Moshitch-Moshkovitz, S., Salmon-Divon, M., Amariglio, N., and Rechavi, G. (2013). Transcriptome-wide mapping of N(6)-methyladenosine by m(6)A-seq based on immunocapturing and massively parallel sequencing. *Nat. Protoc.* *8*, 176–189.
54. Weng, H., Huang, H., Wu, H., Qin, X., Zhao, B.S., Dong, L., Shi, H., Skibbe, J., Shen, C., Hu, C., et al. (2018). METTL14 Inhibits Hematopoietic Stem/Progenitor Differentiation and Promotes Leukemogenesis via mRNA m⁶A Modification. *Cell Stem Cell* *22*, 191–205.e9.